Stable Isotopes in Hailstones. Part II: Embryo and Hailstone Growth in Different Storms

B. FEDERER AND B. THALMANN

Atmospheric Physics ETH, 8093 Zurich, Switzerland

J. JOUZEL

Centre d'Études nucléaires de Saclay, Gif s/Yvette, France

(Manuscript received 17 August 1981, in final form 19 February 1982)

ABSTRACT

Hailstone collections were made in seven storms well documented by radar measurements. Thin sections were prepared of over 2000 hailstones for crystallographic analysis of embryos and growth layers. The majority of the embryos were frozen drops, embedded in a clear layer (2A type). Selected hailstones were also analyzed for their deuterium and oxygen-18 isotope content. The results, plotted in a δD-δO^{18} diagram give information on the extent to which embryos and growth layers evaporated and/or condensed during growth. Frozen drop embryos and clear growth layers showed a significantly stronger evaporation during growth than did graupel and opaque layers. Evidence is presented that some frozen drop embryos are soaked and melted graupel or large aggregates rather than drops formed by coalescence or shed from hailstone surfaces.

Using the isotopic cloud model (ICM) of Part I, an absolute temperature scale was attributed to the isotope values and hailstone trajectories were calculated. The growth ranges of embryos and hailstones are compared with the storms' radar structure. Good agreement was found for most storms, and it is concluded that the ICM gives more realistic results than the adiabatic model used earlier. With the ICM, the large height deviations, obtained with the adiabatic model, are considerably reduced, eliminating the deduction of hailstone growth below −40°C which is impossible. The overall growth range for the 86 hailstones analyzed for D and O^{18} lies between −2.5 and −30.5°C, but hailstones grow *mainly* between −15 and −25°C in a wet mode. The trajectories of the large hailstones are surprisingly flat, indicating that an approximate balance is maintained between updraft and the increasing terminal velocities of the growing hailstones. Measurements of the isotope content of subcloud vapor showed variations of 10–15‰ even on days without precipitation and the crystallographic method for determining δ_0 and thereby fixing the temperature scale is recommended.

1. Introduction

One of the fundamental problems in hail research is the determination of the temperature of origin of hail embryos and of the embryo and hailstone trajectories. Radar Doppler techniques combined with *in situ* aircraft measurements and trajectory calculations have been used to estimate the growth and fallout of embryos and hailstones in three dimensions (Heymsfield *et al.*, 1980; Nelson, 1980). Another approach is the analysis of hailstones collected on the ground, since their properties reflect the conditions under which they were formed in the parent clouds. Various authors have used crystal size and orientation as well as the isotopic composition of hailstones as hailstorm sensors (Macklin, 1977). Both methods yield approximate growth temperatures if a number of assumptions are made, so that rough growth trajectories can be derived (Macklin *et al.*, 1970; Jouzel *et al.*, 1975; Roos *et al.*, 1977; Federer *et al.*, 1978). The most important assumption is adiabatic ascent. Another one is that only dry growth from small cloud droplets occurs, so that the possible formation of a water film on the hailstones' surface by larger drops not in equilibrium with the vapor can be neglected. However, Knight *et al.* (1975) show that during wet growth the isotope content within a particular layer can vary tangentially (variations in the ratio D/H or O^{18}/O^{16} at different azimuths of the same growth layer). Furthermore, in Switzerland and many other places, hailstone embryos have been identified as large frozen drops in a majority of storms, although their exact mechanism of formation is not clear. In both cases evaporation from the liquid water surface can occur. In a classical deuterium-oxygen 18 diagram this is manifested as a deviation from the equilibrium line obtained by Craig (1961) from measurements of natural waters which underwent little evaporation. If evaporation from liquid water on a hailstone surface occurs, an

0022-4928/82/061336-20$09.00

enrichment in O^{18} is observed due to the so-called kinetic effect which arises because of the different diffusivities of the heavy hydrogen and oxygen molecules in air. Measurements of both isotopes on the same samples, which Jouzel and Merlivat (1980) performed, allows the detection of growth layers which underwent rapid evaporation or condensation during growth and the application of a correction for the kinetic effects. Since tangential variations of isotope content are probably due to uneven evaporation from the water film, corrected values should be used to construct trajectories. More importantly, the detection of evaporation effects can contribute another piece of evidence concerning the growth history of embryos and hailstone layers. Specifically, an attempt is made herein to shed some light on the mechanism of formation of frozen drop embryos. Using the isotopic cloud model (ICM) of Part I, the trajectories of a large number of hailstones are deduced and compared with radar data taken at the same time as the hailstone collections were made. The data base of over 2000 hailstones analyzed for crystal and bubble structure (86 of which were also analysed for both D and O^{18}), full radar coverage of the storms in which they grew as well as some isotope measurements in the sub-cloud air providing the storm inflow, is sufficiently large to allow some generalizations to be made on embryos and hailstone growth.

2. Data base and procedure

a. Hailstone classification

Thin sections of 2368 hailstones from seven different storms were prepared. They were all cut parallel to the principal axes of the hailstones. A primary classification was made according to embryo type (graupel or frozen drop embryos). Since the first growth layer is important in the discussion of the embryo growth temperature, the hailstones have also been classified according to the various subclasses given by Federer *et al.* (1978). Table 1 shows the condensed results. A total of 17 different collections were obtained from seven storms on five days, but only three of them were directly quenched in the chilled hexane of the hail collector. The collections from the ground by trained volunteers possibly results in some recrystallization and this must be taken into account in the crystallographic interpretation of these stones (Ashworth *et al.*, 1980). As has been observed in previous collections, most of the storms in Table 1 produced a majority of frozen drop embryos, with the notable exception of the 6 August 1977 storm. An explanation for that will be presented together with these storms' radar structures. Histograms of the subclasses are given in Fig. 1. Hailstones which could not be classified unequivocally amount to less than 15% in all collections (Table 1), and were neglected in this analysis. In all histograms the 1C and 2A modes are pronounced (conical graupel and drop embryos with subsequent clear, large-crystalline layers). This suggests that in all storms both embryo formation mechanisms were at work simultaneously. The classification, which will be discussed further in Section 4, was made after a standardization effort with N. C. Knight of NCAR in our laboratory in September 1978. We can therefore be fairly confident that the interpretations of the hailstone sections given here contain relatively little personal bias.

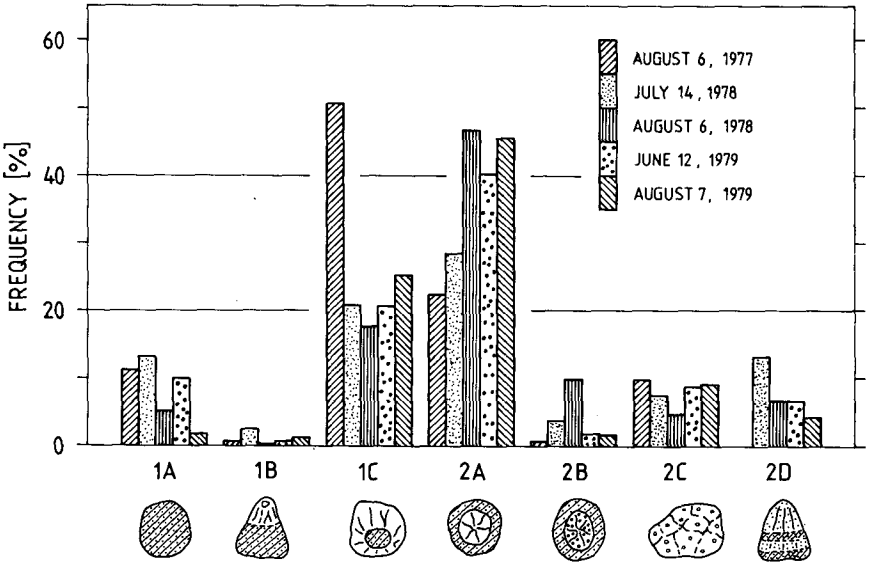

FIG. 1. Frequency distribution of the classified embryos of all hailstones. The classification is that of Federer *et al.* (1978).

TABLE 1. Embryo classification of the hailstone collections from seven storms on five days.

Date (cloud base temperature CCL)	Sampling site*	Sampling mode	Sampling time (CET = GMT + 1)	Diameter interval (mm)	Graupel (%)	Frozen drops (%)	Not classified (%)	Total number	Number analyzed for D, O^{18}
6 August 1977 (6.2°C)	pads Italy N10, M11	ground	1830 h	12–49	62	34	4	71	10
14 July 1978 (10.4°C)	H_1 storm	quenched	1707	3–17	42	44	14	209	
	H_2 storm A	ground	1700	15–27	0	87	13	15	14
	Hergiswil storm D	quenched	1946	8–21	0	87	13	15	
6 August 1978 (9.2°C)	Burgdorf	ground	1815	4–15	42	49	9	195	
	Hofstatt	ground	1830	13–23	36	51	13	55	11
	Buttisholz	quenched	1858	5–17	22	71	7	180	
12 June 1979 (8.4°C)	pads Italy storm B E2	ground	1700	9–25	26	59	15	116	
	D2	ground	1705	4–27	41	52	7	275	
	D3	ground	1705	17–30	27	67	6	70	
	C4	ground	1705	6–29	30	63	7	89	
	C3	ground	1705	8–28	6	82	12	31	
	B4	ground	1708	4–17	37	55	8	369	33
	B5	ground	1710	5–17	33	62	5	309	
	storm D D4	ground	1755	8–18	45	40	15	107	
	D5	ground	1758	8–13	49	36	15	78	
7 August 1979 (10.2°C)	Emmen	ground	1845	6–17	33	59	8	184	18
Total								2368	86

* For a map of the hailpad sites see Cloud Physics Group ETH (1980).

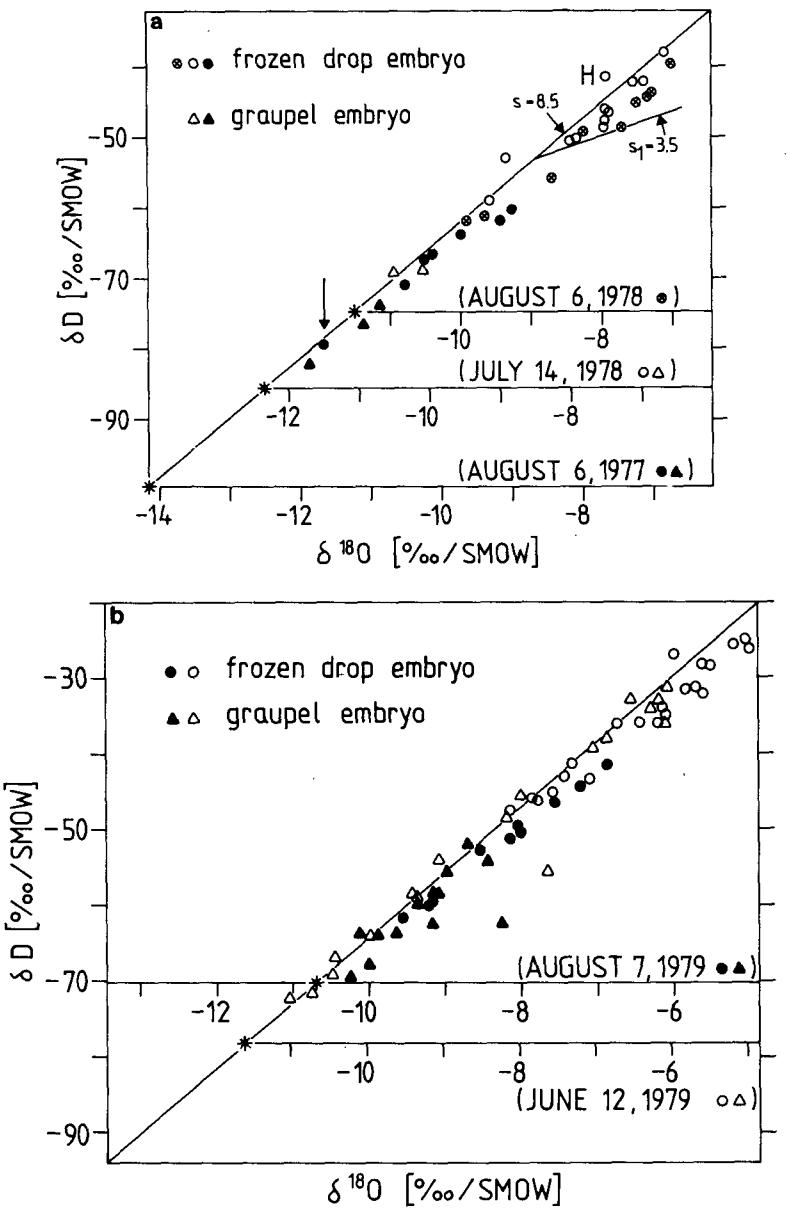

FIG. 2. Deuterium δD (a) and oxygen δO^{18} (b) plots of all the embryos with simultaneous D and O^{18} measurements. The equilibrium line with slope 8.5 is plotted through the points representing the coldest sample of the day (asterisks). The non-equilibrium line with slope 3.5 through a selected point is used to correct the measured isotope values for evaporation effects. The arrow marks the absolute coldest frozen drop embryo.

b. δD-δO^{18} measurements

A total of 86 hailstones were analyzed for their isotope content [determination of the ratios $C = HDO/HHO$ and H_2O^{18}/H_2O^{16} (ppm) or the deviation from the standard mean ocean water SMOW (‰): $\delta = (C/C_{SMOW}) - 1$; 1 ppm = 6.42‰ for deuterium]. Three to eleven samples of ~20 mg were cut from different growth layers of a section ~3 mm thick and analyzed in the mass spectrometer at Saclay for D and O^{18} simultaneously (Jouzel and Merlivat, 1980). The standard deviation of the measurements on the smallest samples are $\delta_D = \pm 0.5‰$ and $\delta_{18} = \pm 0.15‰$ of SMOW. A convenient presentation of the data are the δD-ΔO^{18} plots in Fig. 2 where the D and O^{18} concentrations of the embryos of all the hailstones are indicated. A detailed description of the plots is given by Dansgaard (1964). Briefly, the sta-

ble isotopic composition of most meteoric waters not subjected to extensive evaporation have a linear relation best described by

$$\delta D = s\delta O^{18} + d_0 , \quad (1)$$

where $s \approx 8$, and d_0, the so-called deuterium deficiency is ~10‰ (Craig, 1961; Dansgaard, 1964). It was checked whether the same linearity existed in the calculated isotope contents of hailstones over the temperature interval 0 to −35°C. The slopes were $s \approx 8.5$, slightly higher than those found in waters on a global scale. A value of $s \approx 8.5$ is obtained for all the storms considered and independent of the choice of the parameters used in the cloud model.

For non-equilibrium processes (rapid evaporation and condensation), a kinetic effect due to the differences between the molecular diffusivities of the three water species (H_2O^{16}, HDO and H_2O^{18}) must be taken into account. This kinetic effect changes the δD-δO^{18} slope abruptly to as little as $s_1 \approx 3.5$ (Merlivat and Jouzel, 1979). Thus, if non-equilibrium effects occur, the liquid collected by a hailstone which initially lies on the equilibrium line, starts to vary along a line with slope 3.5. For the interpretation of hailstone trajectories it is interesting to deduce the effect of the correction obtained by projecting the measured δD values along s_1 on the equilibrium line. This is done because the equilibrium δD of the droplets responsible for the accretion is of interest in determining the temperature/height of the particular growth layer. The effect is small and can usually be neglected. In Fig. 2 the equilibrium lines with slope $s = 8.5$ are drawn through the coldest opaque samples of the day, which theoretically should be those exhibiting a minimum of non-equilibrium effects.

3. Deduction of the height of formation of hailstone growth layers

a. Means of fixing the temperature scale

There exist three methods to estimate the isotope content, δ_0, of the vapor feeding the cloud and to assign a temperature scale to the isotopic variations. Here we shall briefly describe each method, while the procedure used for each day is discussed in Section 4. Macklin *et al.* (1970) estimated δ_0 by attributing the extreme values of D and O^{18} measured in hailstones to growth temperatures of −35 and 0°C. In this way a relationship between δ_0 and the D content, δ_c, of the condensed phase is obtained by calculating the height profiles of saturation mixing ratio and condensed water related to temperature through the adiabatic assumption. Since in the ICM, described in Part I, the D content of hail, δ_H, results from the interaction of five water species, no simple analytical relation exists between the isotope content of the hailstone layers δ_H and δ_0. Therefore, a trial and error method has been employed. First a reasonable δ_0 is estimated using the adiabatic assumption. Then, using the model, an approximate δ_H profile is calculated. The D concentration corresponding to a specific extreme temperature or, better, identified from crystallographic analysis is compared with the results of the first approximation. According to Levi and Aufdermaur (1970) large crystals (>2 mm) grow at $T_c > -24$°C and small crystals (<0.5 mm) at $T_c < -15$°C. The small-crystalline layer with the highest isotope content of the day was attributed to a growth temperature of −15°C and the large-crystalline layer with the lowest isotope content to −24°C. Crystal size in the thick sections used for isotopic analysis was obtained from measurements in adjacent off-center thin sections, if the hailstone diameter was larger than ~25 mm, and estimated from the opacity of the thick sections or from thin sections of similarly structured hailstones in the collection, if the diameter was smaller than 25 mm, which was often the case. Since the correlation between opacity and the two classes of crystal size was high (see Section 6), this method of the temperature "fork" seems to give satisfactory results. A precise, direct determination of crystal size in the hailstones analyzed for the isotopes is not possible and has not been made in the off-center thin sections either. The reason for this was that many hailstones were recrystallized, so that detailed quantitative deductions are not warranted (Ashworth *et al.*, 1980). The temperature "fork" yields two δ_0 values. To obtain the final δ_0, the δ_H profiles were shifted in such a way that all the hailstone layers in the collection were consistent with the growth temperatures obtained. This final δ_0 takes all the layers into account and no growth temperature deduced from the isotopic measurements contradicts crytallography. It yields the optimum δ_H profile as well as the D profile of the entrained vapor δ_e, by using either the average decrease $d\delta_e/dz = 3.9$ ppb m^{-1} of Ehhalt (1974) or the smaller one of 2.0 ppb m^{-1} just below cloud base (1.5–2.1 km), which is the average measured in the experiment described below. In any case it must be assumed that the subcloud vapor has constant isotope content both in time and space. Some aircraft measurements from the United States have shown that this assumption was not justified, even in the one case where uncontaminated inflow air was sampled at cloud base (Knight *et al.*, 1981). The third method of determining δ_0 is the measurement of subcloud vapor during prestorm conditions. The reliability of this method has been investigated on a mountainside by sampling vapor simultaneously at five stations from 430 to 2100 m MSL. The five stations were equipped with cold traps cooled in a chilled hexane bath. The airflow was adjusted to 2 L min^{-1} in order to freeze out all the water vapor passing through the trap so that no fractionation of HDO and H_2O^{18}

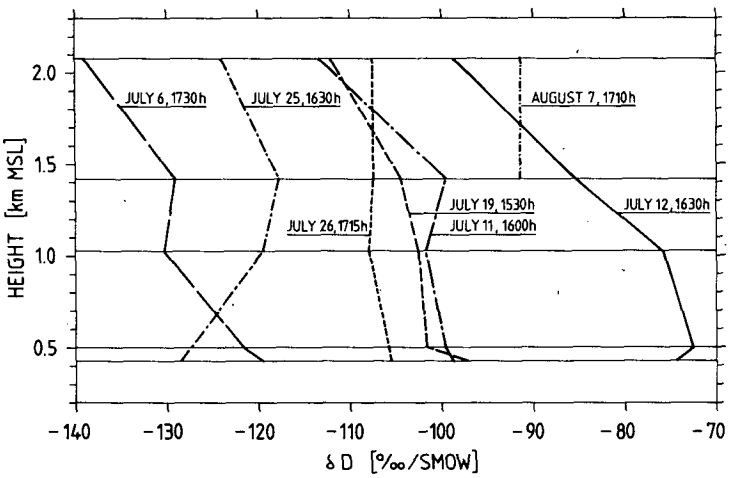

FIG. 3. Profiles of D content of subcloud water vapor as a function of altitude for various days in 1979. The 12 July samples were taken after rain. The 7 August measurements were made 95 min before the hail collection (Table 1).

could occur. At the same time the temperature and dew point of the ambient air was recorded. A comparison was made of the mass of water vapor sampled to the mass expected in the sampled air volume. Samples where the difference was larger than 20% were discarded. The detailed results are listed in Cloud Physics Group, ETH (1980).

During 1978 and 1979 a total of 153 vapor measurements were obtained and a selection of D values as a function of altitude is indicated in Fig. 3. In prestorm conditions one would assume that the boundary layer is well mixed up to about cloud base height (~2 km in our area). The almost vertical profiles on the two storm days (26 July and 17 August 1979) support this assumption. Otherwise the D values varied appreciably on almost all days. The most salient feature of Fig. 3 is the general decrease of δD (and also δO^{18}) above 1500 m. This gradient amounts to 0.013‰ m^{-1}. In the lowest 1000 m, where most of the inflow air originates, the gradients are generally less, but even on days with light precipitation 3 h before sampling (6 July), the deviation can reach 11‰. The time variation at the same sampling site also varied by about 11‰ in 2 h. The horizontal variation was even larger. Typically, simultaneous measurements gave a difference of ~13‰, but extreme values up to 22.5‰ over 35 km were observed. The latter measurements, however, were made by the Italian crew in a narrow valley, where local vapor sources might have influenced the measurements.

This experiment showed that δ_0 can vary a great deal at subcloud levels, which of course renders the interpretations of isotope measurements in terms of absolute temperature difficult. For the present purposes we will use crystallography or the method of extreme values except for 7 August 1979 and compare the results with vapor measurements when they are available.

b. Evaluation of the deductions in terms of consistency of crystallography and isotopic methods

The general classification of the hailstones according to embryo type is given in Table 1, which shows that it is justified to distinguish between storms in which either the graupel or the frozen drop mechanisms dominate. It has been observed by Knight and English (1980) that embryo type varies within a hailswath, so that the commonly indicated dominant mode may depend on the location of the collection with respect to the storm center. A comparison in Table 1 of the seven collections in storm B of 12 June 1979 reveals that the dominant embryo type remains the same if collections from the center and the periphery of the hailswath are compared. The other storms show the same result. A stratification according to large (radius $r > 7.5$ mm) and small hailstones does not change the above observation except for the 6 August 1977 storm. Here, contrary to most other observations, the larger stones have predominantly graupel embryos, while the embryos of the smaller ones are frozen drops. Three collections were obtained on 6 August 1978, of which the first two were not quenched. The extreme sizes were about the same in the three collections, but the percentage of rimed embryos decreased considerably over the 40 km path (see Table 1). A total of 86 hailstones have been analyzed for their stable isotope content. Typical hailstones which are representative for each collection have been chosen for discussion (interesting exceptions will be discussed below). Examples are shown in Figs. 4–9. In addition, the δD and δO^{18} values are plotted as a function of hailstone

radius. Note that growth altitude increases with increasing $-\delta D$ and $-\delta O^{18}$. In these plots the δO^{18} ordinate corresponds to the δO^{18} equilibrium values lying on a straight line according to Eq. (1) with slope $s = 8.5$ through the coldest sample of the day. The deviation Δ of δO^{18} from the equilibrium line can be expressed by

$$\Delta\delta O^{18} = (8.5\delta O^{18} - \delta D + d_0)/5, \qquad (2)$$

and is a measure of non-equilibrium evaporation ($\Delta\delta O^{18} > 0$) and condensation effects ($\Delta\delta O^{18} < 0$). The standard deviation of $\Delta\delta O^{18}$ for individual points according to (2) and Section 2b is $[(8.5 \times 0.15)^2 + 0.5^2]^{1/2}/5 = 0.27‰$. If the measured $\Delta\delta O^{18}$ is larger than this value, it can be assumed that the evaporation/condensation effect of the particular layer is significant. In Figs. 4–9 the distance between the δD and the δO^{18} values is proportional to $\Delta\delta O^{18}$. Layers which evaporated have a positive δO^{18} value (broken lines) lying below the δD value. Taking the coldest sample of the day as a reference for the equilibrium isotope values gives a lower limit for the extent of evaporation. However, if in a larger collection of hailstones, a still colder sample would have been found, the condensation effects would become smaller. Therefore, evaporation with $\Delta\delta O^{18} > 0.27‰$ are considered significant, whereas condensation effects are more uncertain.

In Fig. 4 a typical large hailstone (1C type) is shown (see also Fig. 1). After the graupel has grown to ~15 mm, starting from its tip (designated by E in Fig. 4), it started to grow a layer with D values between −90 and −95‰ on all sides. This means that the graupel began tumbling and, at later stages, assumed another stable fall direction perpendicular to the graupel axis. Note the almost perfect correspondence of the isotope values at the two outer boundaries. Hailstones in this collection with $r > 12.5$ mm and graupel embryos show the various transition stages from conical to oblate and to almost perfectly spherical. The frozen drop embryos produced hailstones with many transitions from clear to opaque ice, while the stones that grew from graupel embryos are mostly opaque. A typical hailstone of 14 July 1978 is shown in Fig. 5. In this storm the 2A type frozen-drop embryos are the most frequent ones. From crystallography a simple upward trajectory is indicated. The isotope data of this quenched hailstone, which is from collection site H_1, imply a fall to higher temperatures after the embryo stage and then a rise. The deviation of the O^{18} content of the embryo from the equilibrium value shows condensation (see also Fig. 2). Apparently, a large cold particle descended into warmer regions, thereby growing by condensation/deposition. It was then injected into a wet updraft, heavily soaked and carried to higher altitudes while growing (partly in a spongy mode, as seen in the shades of the clear layer of the quenched sample). This suggests a clear separation between embryo and hailstone growth, a fact suggested by the radar pattern in Fig. 21. Note also that the tangential variations in this hailstone (and in many others) are not very large. From the same collection a typical quenched graupel (hailstone O) is shown in Fig. 6. The opaque tip and periphery condensed, but the clear and spongy middle layers were evaporating at an exceptional rate. In this hailstone the injection into a wet updraft and ejection at higher altitude is well demonstrated.

In the 6 August 1978 storm the 2A type hailstones were the most frequent ones as well. In Fig. 7 a

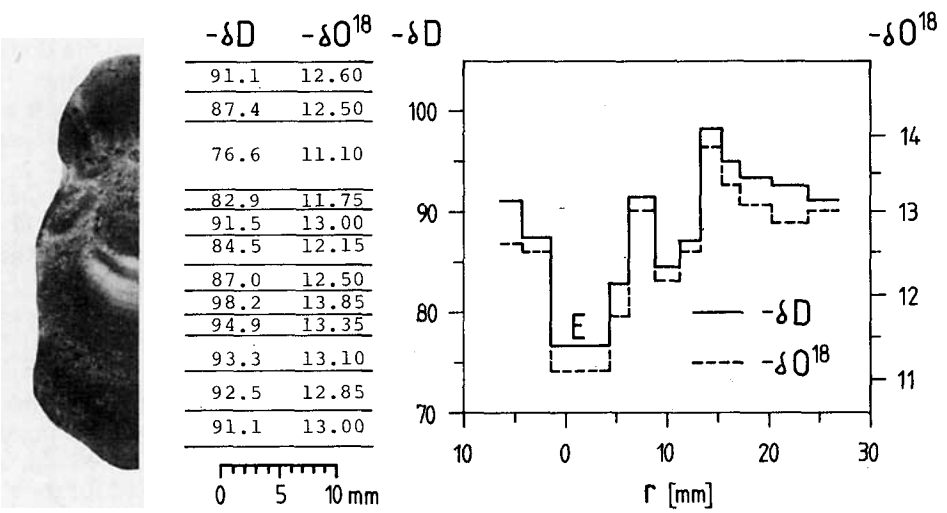

FIG. 4. Thick section and isotope data as a function of radius for hailstone D (1C type) of the 6 August 1977 storm. The embryo is designated by E. The δD (full line) and δO^{18} (broken line) scales are matched according to the equilibrium line with slope 8.5 in Fig. 2, so that the difference between the two lines is a measure of evaporation/condensation effects.

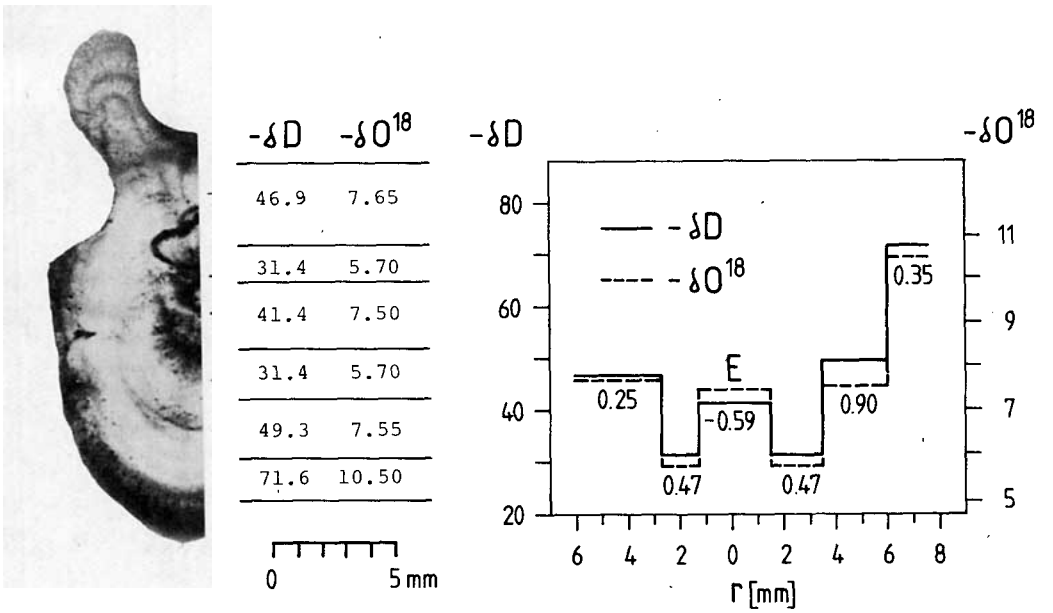

FIG. 5. As in Fig. 4, except for 14 July 1979, hailstone H, which was quenched. The embryo is a transition between a graupel and a frozen drop. The numbers indicate values of $\Delta\delta O^{18}$ (see text).

typical quenched example is shown. As expected, the embryo surface evaporated and also the subsequent clear layer which has traces of spongy growth. The outer opaque layer, which grew at high altitudes, also evaporated strongly. This suggests that, contrary to the situation in Fig. 6, the layer became wet on descent. A large hailstone of 12 June 1979 in which 11 layers were analyzed, is depicted in Fig. 8. The O^{18}-poor opaque layers at 8–9 mm from the center of the frozen drop embryo are followed by clear layers relatively rich in O^{18}. This indicates a descent to warmer temperatures, whereby water vapor condensed on the surfaces of the opaque layers. Since this hailstone is from the largest collection, the condensation effect is probably real, but its absolute value is still uncertain. Such condensation is only detectable if no further accretion of droplets occurs during descent. It is possible that during this period

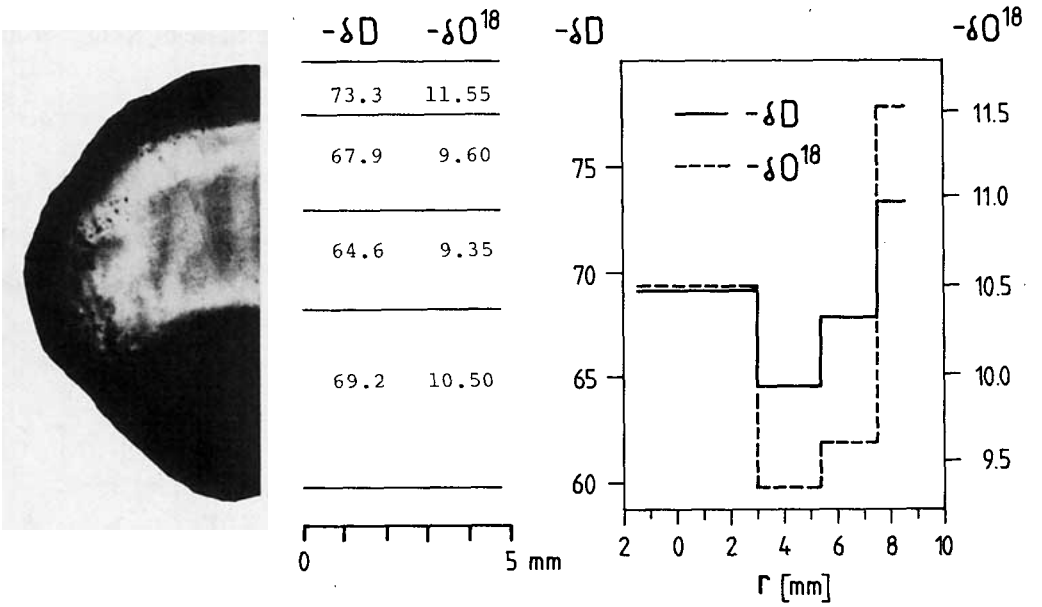

FIG. 6. As in Fig. 5, except for hailstone O (quenched 1C type).

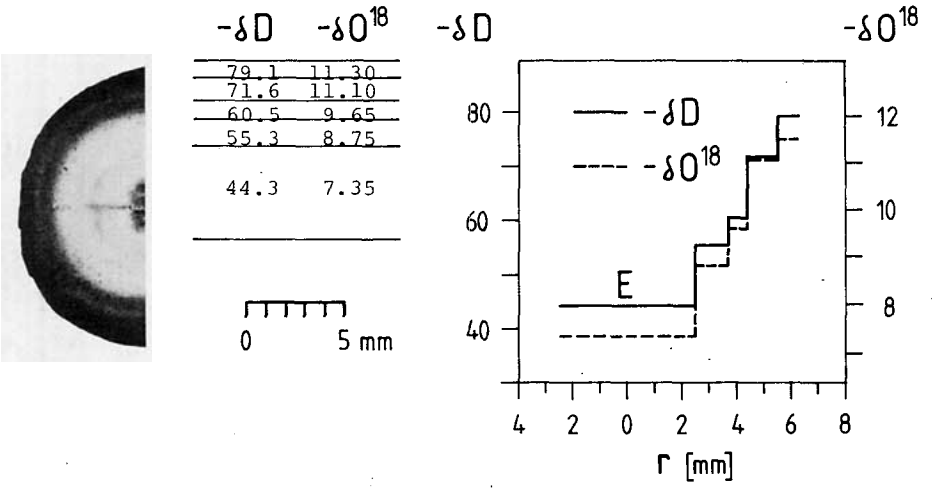

FIG. 7. As in Fig. 4, except for hailstone N (quenched) of the Buttisholz-Collection on 6 August 1978 (2A type).

the hailstone fell in air which was relatively dry. This is a general observation for descending trajectories of embryos and growth layers, but not necessarily for the final fallout.

A typical 2D-type hailstone of the 7 August 1979 storm is given in Fig. 9. The embryo is a half-sphere, which are found quite frequently in certain storms. Layers of this and most of the other stones analyzed show irregular protrusions, indicating growth in a very wet environment. Judging from the small range of D values given in Fig. 9, the hailstone was nearly balanced during its growth.

4. Trajectories

In this section the trajectories deduced from the isotope data are discussed. A rough idea of the form of the trajectories can be obtained from the original $\delta D/\delta O^{18}$ data in Figs. 4–9. To attribute an absolute temperature scale to the isotope data, two methods are available: the simple adiabatic model (AM), and the new isotopic cloud model (ICM) presented in Part I. Emphasis is placed in this section on a comparison of both models. In a first step, the D content of the vapor feeding the cloud must be determined. As mentioned previously, three procedures are available: 1) determination of the extreme D values and attributing these to growth temperatures of 0 and −35°C; 2) determination of the minimum D content in layers with large crystals, of the maximum D-content in small-crystalline ice, and attributing these to −24 and −15°C respectively; and 3) vapor measurements in the subcloud layer. Considering the results of Section 2 and those of Knight *et al.* (1981),

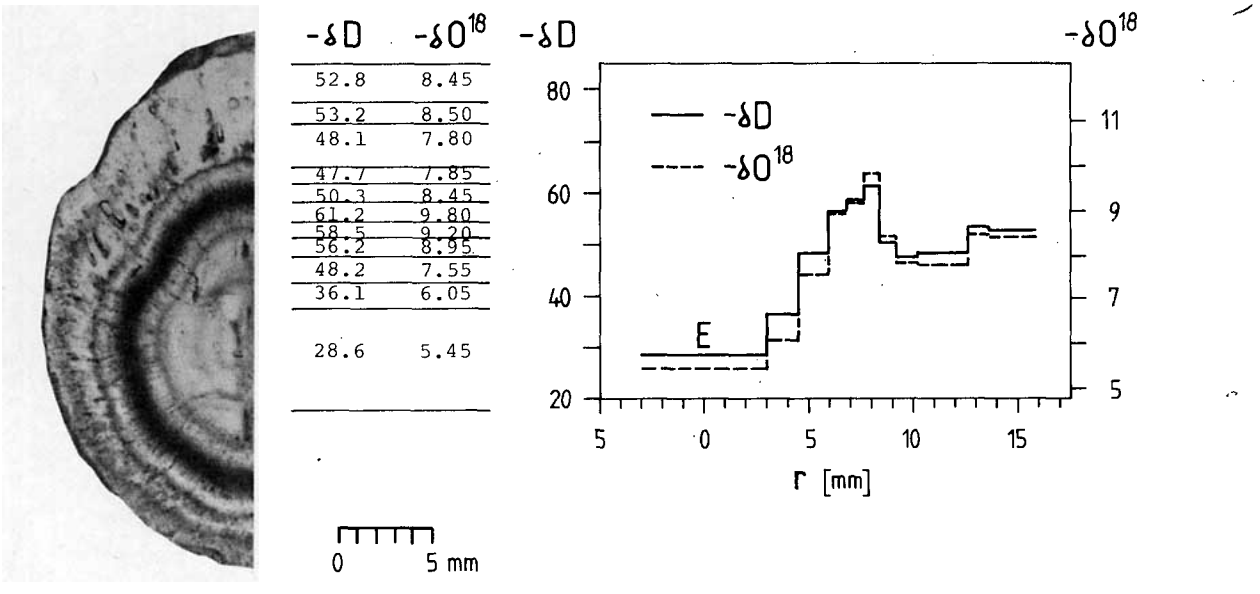

FIG. 8. As in Fig. 4 except for hailstone A of 12 June 1979, storm B (2A type).

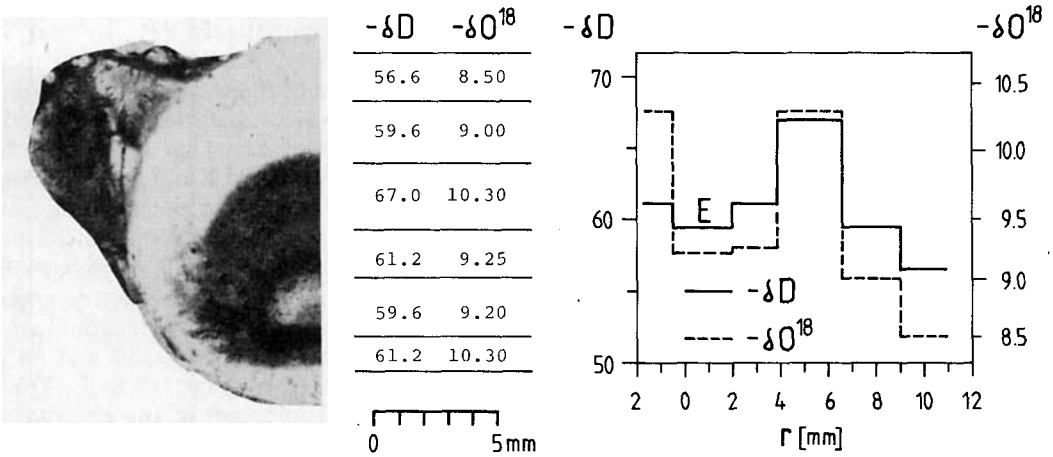

FIG. 9. As in Fig. 4 except for hailstone P of 7 August 1979 (2D type).

we feel that not too much weight should be attached to the vapor measurements. The method of the extrema cannot be used if growth takes place in a relatively narrow D range (as in the 7 August 1979 storm) or if only a few samples are available. Since the correlation between bubble structure and crystal size is exceptionally high [especially the one between large crystals and clear ice (see Section 6)], substantial confidence in the use of the temperature "fork" (method 2) is probably warranted.

Trajectories of the hailstones depicted in Figs. 10–14 were determined using the $\delta_H - T_c$ relationship, calculated for 5 days in the same way as the examples given in Fig. 4 of Part I. δ_H is the calculated D content of the hail, taking into account its interaction with droplets (δ_c), ice crystals (δ_i), raindrops (δ_r) and large ice particles (δ_g), which all have either a direct influence on the growth process or an indirect one on the remaining vapor (δ_v). The trajectories based on the AM were also determined in the usual manner and using the same δ_0 as for the ICM.

The growth ranges obtained from the entire set of measurements for each day are also displayed in Figs. 10–14. It is seen that the ICM gives smaller growth ranges than the AM and very flat trajectories, indicating balanced growth over a considerable time period for the larger stones in Figs. 10, 13 and 14. This is in line with model calculations of Nelson (1980). If the growth ranges are based on the AM, the lowest growth limit is placed at or below $T_c = -40°C$ on all days except 080779. Since for various reasons growth below about −30°C is slow or absent (Macklin, 1977), this result seems unrealistic. Taking into account the uncertainty in δ_0, the range could simply be shifted toward warmer temperatures. But this is in conflict with the deductions from crystal size and it is difficult to accept exceptionally warm growth layers in so many cases. On 071478 such a correction would result in a warm growth limit which is at a positive temperature [see also Roos *et al.* (1977) for a discussion of this problem]. With the trajectories and growth ranges based on the ICM, no such problems are encountered.

If these trajectories and maximum growth ranges are compared with the radar data in Section 5, a rather good correspondence between growth heights from Figs. 10–14 and the heights of the higher reflectivities is obtained. A notable exception, however, is the ICM trajectory of hailstone D in Fig. 10. The $\delta_0 = -105.7‰$ was determined using the temperature "fork." A δ_0 calculated from the extreme values yields −106.98‰. The higher trajectory with more pronounced height deviations, based on the AM, seems to correspond much better to the high reflectivities up to ~12 km depicted in Fig. 20 (see the small E and H growth ranges, based on the ICM, in comparison with the RHI pattern). Undoubtedly, relatively large particles were present up to and above the tropopause (11.3 km), as indicated by the X-band radar. But whether they were actually growing from 1.5 to 2.5 km above 9 km is doubtful. It seems that the ICM gives more realistic trajectories in this storm as well, since the special conditions that

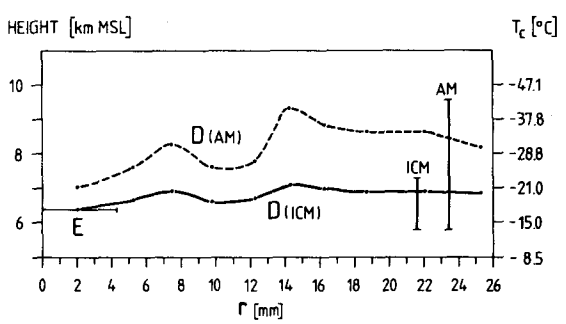

FIG. 10. Trajectories of hailstone D of the 080677 storm derived from the adiabatic (AM) and the isotopic cloud model (ICM), respectively. The growth ranges for the entire collection on that day are also indicated for both models. The embryo is indicated by E.

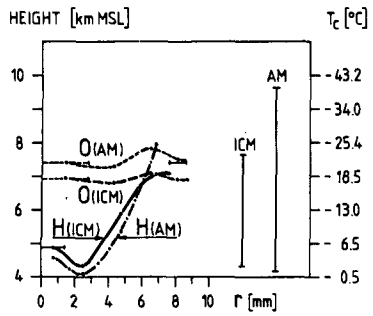

FIG. 11. Trajectories of hailstones O and H of 14 July 1978. H and O (ICM) are based on the isotopic cloud model, O and H (AM) on the adiabatic model.

would have to be met to explain the AM trajectory are probably not real.

A case of embryo recirculation is shown in Fig. 11 for hailstone H. The condensing and falling embryo of Fig. 5, which seems to be an aggregate formed in the overhang (Fig. 21), is injected into the tilted updraft and finally thrown out at 7.1 km. Growth in this updraft is very wet, as shown by the traces of a sponge and the evaporation in Fig. 5. The trajectories in Fig. 11 were calculated using the extreme temperature values (0 and −35°C) with δ_0 = −90.3‰ for D and −12.1‰ for O^{18}. These values are very close to the mean of the three vapor measurements on that day ($\bar{\delta}_0$ = −89.6‰). From the same collection the trajectories of hailstone O, whose thick section and isotope data are depicted in Fig. 6, are drawn in Fig. 11. Both trajectories based on the ICM and AM, respectively, are consistent with crystallography and radar data. Generally, however the range of growth temperatures from the AM is very large in this collection, and more confidence is placed again into the ICM. The graupel embryo of hailstone O was condensing while falling slightly. The subsequent layers are seen to grow wet with extensive evaporation and becoming spongy, while the outermost layer is again condensing strongly. The evaporation of the clear layers in the middle of the growth trajectory is characteristic for many hailstones in this collection. This suggests that their surface was considerably warmer than the ambient temperature. This could be due to accretion of relatively large droplets which are not in temperature equilibrium with the environment. The trajectory of O is remarkably balanced, probably because the graupel embryo grew close to the main updraft. The embryo of hailstone H, on the other hand, may have descended first to 4.3 km where it was probably heavily soaked while recirculating. Although the height of origin and the type of both embryos could be the same, embryo H is classed as a frozen drop (Fig. 5). Both hailstones had the same end point on the ground but their fallout history from 7 km is different. In contrast to H, hailstone O has a periphery which was condensing strongly. This shows that it fell in a downdraft which was relatively dry, so that no more growth was possible. Otherwise, the condensation effect would have been masked. The outermost layer of hailstone H was evaporating and formed a characteristic protuberance which could be interpreted as icicle lobe (Knight and Knight, 1970). Apparently a liquid layer was freezing preferentially at the tip in slightly wet growth from droplets of 15 μm radius.

In the 6 August 1978 and 7 August 1979 storms no evidence of embryo recirculation is apparent. In Fig. 2 no signs of embryo condensation can be seen for those two storms, and Figs. 12 and 14 together with the radar pattern (Figs. 19 and 23) suggest a rather horizontal injection of the embryos into the main updraft. In the storm of 080779 the growth interval is exceptionally narrow on the basis of both models. Fortunately there were two vapor measurements at different altitudes available to determine δ_0 (Fig. 3), which yielded almost the same value (δ_0 = −91.5‰). The trajectories are consistent with the radar pattern and crystallography. This storm was weak and produced large quantities of small hailstones.

The largest sample analyzed for isotopes was obtained from the seven collection sites in storm B of 12 June 1979. Most trajectories indicate that the hailstones encountered multiple updrafts and were therefore able to grow to relatively large sizes. The δ_0 was determined from crystallography. Due to the large sample the temperature "fork" reduced the possible range for δ_0 considerably, namely, δ_0 = −81.2‰ for the layer richest in D with small crystals and δ_0 = −77.8‰ for the layer poorest in D with large crystals. There were two distinct groups of graupel embryos: 1) those which had a warm origin, similar to the frozen drop A in Fig. 13 (which often showed signs of soaking and melting of rimed particles) and 2) those which originated at higher levels like the graupel in hailstone N of Fig. 13. The latter remained small and conical. This situation leads again to the speculation that all embryos originate in the same general region, but some are directly injected into the updraft at low temperatures and

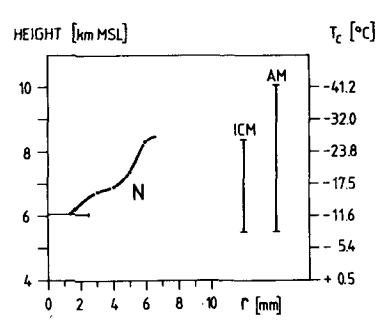

FIG. 12. Trajectory of hailstone N from the 080678 collection at Buttisholz, calculated with the ICM.

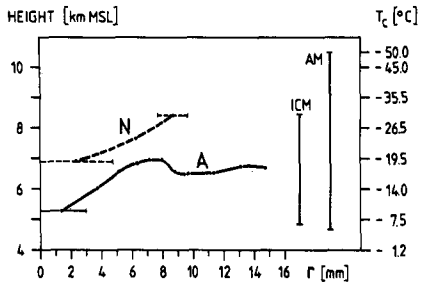

FIG. 13. Trajectories of hailstones N (1C type) and A (2A type) of the 12 June 1979 storm calculated with the ICM.

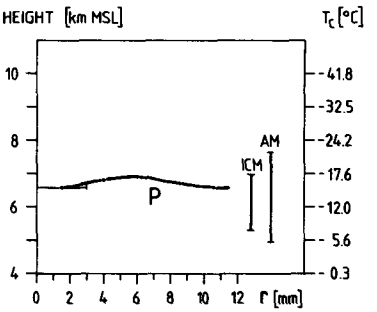

FIG. 14. Trajectory of hailstone P from the 7 August 1979 storm.

others at high temperatures and recirculated. The latter can be transformed to such an extent that they are classed as frozen drop embryos. Some such transition-embryos were observed and a typical example is shown in Fig. 15. The bubbly center still has a conical appearance surrounded by a clear and a transparent layer. The embryo was classified as a graupel although it is at the warm extreme. The layers out to the large radial bubbles (marked by a change in illumination, introduced artificially), are evaporating and the subsequent layers slightly condensing. Two other graupel embryos, somewhat less transformed by soaking and melting, were among the sample analyzed for isotopes. They both had intermediate δD values between the richest and the poorest layers of the parent hailstones, which supports the embryo recirculation hypothesis. The collection of 12 June 1979 gave trajectories with small height deviations of hailstone growth and in good agreement with the radar pattern in Fig. 22, if the ICM was applied. Using a mean $\delta_0 = -78.7‰$, the AM gave a growth interval extending down to $T_c = -50°C$ which is unrealistic. Even if the scale is moved by 6.5°C to start at 0°C (Fig. 13), the obvious contradiction can only be resolved by assuming a variation of δ_0 for the colder hailstones. This possibility cannot be ruled out, however, since hailstones with the coldest layers ($\delta D < -65‰$) fell exclusively at the northwest edge of the hailswath (hailpads B4 and B5 in Fig. 22). There they might have encountered updraft branches feeding from subcloud air with different characteristics in that mountainous region.

5. The storms

All the seven storms described below occurred within the range of the two meteorological radars at Emmen AFB, where the operations center of Grossversuch IV is located (Federer *et al.*, 1979). Low-level PPI's in 1 min time resolution are available from the S band radar. The spatial resolution is 1° in azimuth and 330 m in range. Color film with 5 dB(Z) steps was used for the analysis. The vertical sections (RHI's) are obtained at irregular intervals (20 s to several minutes) from the X band radar, which is primarily dedicated to the seeding operation (Waldvogel *et al.*, 1979). Wind information on a continuous basis was available from the four stations in the experimental area indicated in the figures below. The radar data of the storms are analyzed with a view to deriving information about the character of the storms and cells during the collection periods and the location of the main updraft. A cell is defined by a local precipitation maximum [usually 55 dB(Z)] presumably produced by a convective updraft-downdraft pair. Special attention is given to the detection of radar echo features that may indicate particles serving as hailstone embryos. In the analysis, the classical picture of a two-stage process in hail formation, embryo growth and subsequent hailstone growth in a different environment was kept in mind. Since only Z values and environmental winds from the 1200 GMT radiosondes are available at levels above cloud base, the conclusions concerning the

FIG. 15. Thick section of a hailstone whose graupel embryo is substantially transformed by soaking and/or melting. The D and O^{18} measurements show that evaporation takes place out to the layers marked by the change in illumination, introduced artificially. The outer layers show condensation.

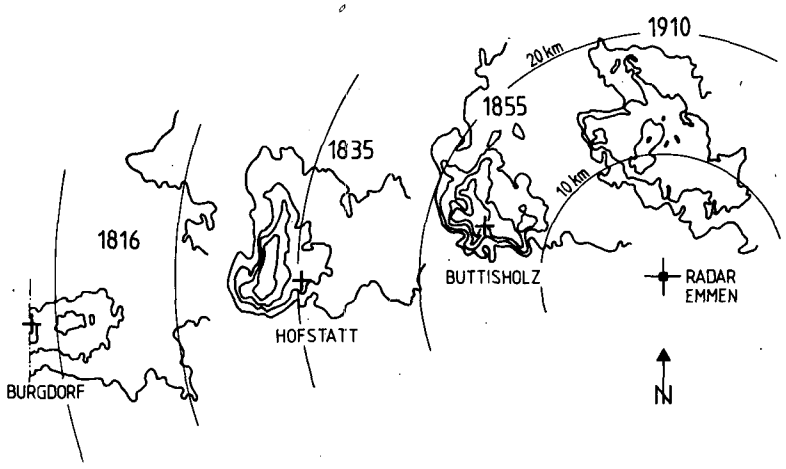

FIG. 16. Radar echo structure at large scale for the 6 August 1978 storm. The collection sites with respect to the radar echo are indicated by crosses. The contours are S band Z values of 30, 45, 55 and 60 dB(Z) at an antenna elevation of 5° (1816 CET) and 8° (1835, 1855, 1910 CET). Central European Time (CET) = GMT + 1 h.

cloud kinematics are somewhat speculative. The degree of speculation can be judged from the following example which will be given in detail. The remaining storms of the other four days will be presented only summarily by means of a typical radar picture which best represents the general situation.

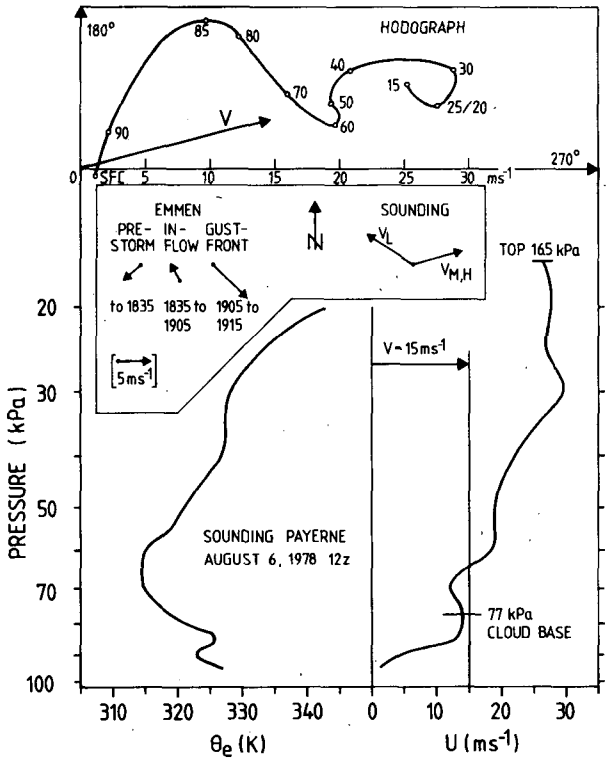

FIG. 17. θ_e profile and wind component in the direction of storm movement for 080678. The insets show wind vectors at the radar site during the passage of the storm and the low, mid and high-level ambient winds relative to the storm movement and the hodograph; V is storm motion.

a. 6 August 1978

In the strong southwesterly flow ahead of a pronounced trough extending from western England to Spain, a wave proceeded rapidly toward central Europe, advecting colder air. The front reached the experimental area in the late afternoon. Its passage lead to widespread thunderstorm activity on the Swiss Plateau. The storm from which hailstone collections were made was associated with this passage of the front. It originated outside the area covered by the radars and was already producing hail when it entered the area (Fig. 16). This storm was relatively steady during the hail collections. It moved at 15 m s^{-1} parallel to the cloud layer winds, thereby overtaking the low-level winds. In Fig. 17 the θ_e profile of the prestorm environment is indicated together with the horizontal wind component in the direction of storm movement. It is seen that the storm velocity is such that at low levels (up to ~65 kPa) the unstable air flows into the storm from 110°, i.e., at the right forward flank of the traveling storm. The wind vectors relative to the storm in the subcloud layer $\mathbf{V_L}$, middle troposphere $\mathbf{V_M}$ (cloud base to 30 kPa) and upper troposphere $\mathbf{V_H}$ (to 15 kPa) were calculated after Newton and Fankhauser (1964) from hodographs, of which an example is also given in Fig. 17. Storm motion V is from 253° at 15 m s^{-1}. Note also the wind shifts at the radar site. During the passage of the storm, 10 km to the northwest of the radar (Fig. 16), the flow is toward the storm from 1835 to 1905 (all times GMT), and at 1905 a strong gust front reaches the radar site. The radar echo structure at 1835 during the second hail collection

shows a persistent weak echo region (WER) on the southern flank of the storm (Fig. 18). A strong echo of over 50 dB(Z) is present at 7 km in the RHI along A-A. This echo is located to the south and outside both 30 dB(Z) contours of the 5° and 8° elevations superposed in the lower panel. This echo structure indicates a strong organized updraft on the southern flank of the storm. A WER is still present during the third hailstone collection at 1855, as shown in Fig. 19. The echo-free area [<20 dB(Z)] beneath the maximum reflectivity at 6 km in section A-A of Fig. 19, and the pronounced overhang in both vertical sections, support the view that embryos are growing in the overhang and are then injected into the strong updraft where they grow to hailstone size and produce the intense echo aloft and the hail cascade to the north of the updraft seen in the PPI's of Fig. 16. In Fig. 19 the ballistic and parachute trajectories of rocket W22 fired at 1854 are also shown. The parachute, carrying the empty rocket, opened in the strong reflectivity gradient at a height of 4.6 km beneath the area of 50 dB(Z) at the −10°C isotherm (stippled), which is forming the overhang and landed 21 km further downwind. With a fall velocity of 7.5 m s^{-1} for the empty rocket, such a parachute trajectory is only possible if the parachute opened in a strong updraft. This observation corroborates the interpretation of the radar pattern. After 1910 part of the updraft area on the southeast side of the main echo begins to be filled with particles (see Fig. 4) and the WER disappears. At the same time hail production stopped as documented by the hailpad data, but whether the massive seeding influenced the WER is difficult to say. This was a multicell storm with new growth originating on the southern flank and increasingly mature cells travelling through the storm and dying in the northern part. The hail pattern on the ground also reflected the storm's pulsations.

In Figs. 18 and 19 the range of embryo and hailstone growth as deduced from the isotopic analysis is also indicated. Taking into account the limits of accuracy of radar heights and isotopic data, the agreement between strong reflectivities and the growth ranges in the overhang (embryo formation zone) and above the main updraft (hail growth zone) is very satisfactory. This observation lends considerable credence to both the radar and isotope interpretations.

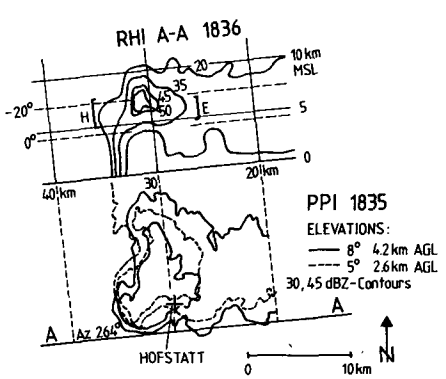

FIG. 18. Radar echo structure of the 6 August 1978 storm during the second hail collection. The range of embryo (E) and hailstone growth (H) deduced from isotope data in conjunction with the ICM is indicated in the RHI (A-A).

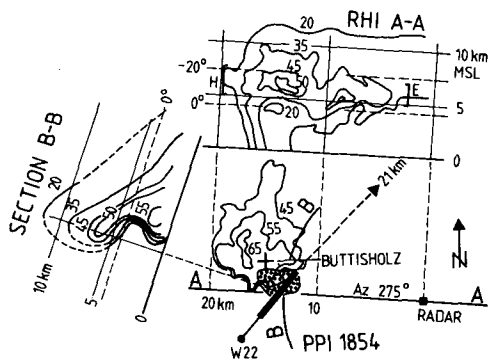

FIG. 19. As in Fig. 18 except for 1854 CET during the third hail collection.

b. 6 August 1977

In this storm, which is depicted in Fig. 20 at the time of the hail collections, low-level air enters the main updraft on the northern flank of the intense echo from 030° (see wind vectors relative to the storm in the inset). The organized updraft produces a persistent WER and overhang from 1825–1910. The seeding criterion was met from 1812–1935. Ice crystals are formed above this updraft at temperatures lower than −20°C and either enter the anvil or grow in the forward overhang, where they give rise to a relatively strong echo [>40 dB(Z)]. The anvil and overhang are reminiscent of the supercell model of Browning and Foote (1976). In the overhang, which extends over a considerable temperature interval, ice crystals from the anvil apparently meet favorable riming conditions for an extended period of time. This results in the predominance of graupel embryos in this storm. From the overhang they can be recirculated into the main updraft where they are transported rapidly to high altitudes thereby growing to hailstones. The reflectivities > 45 dB(Z) at temperatures below −40°C indicate the presence of large particles at these levels. The ICM gives very narrow embryo and hailstone growth ranges, which differs considerably from those expected on the basis of the radar pattern (see Section 4).

c. 14 July 1978

Numerous vertical sections and PPI's at two antenna elevations of storm A suggest that the storm

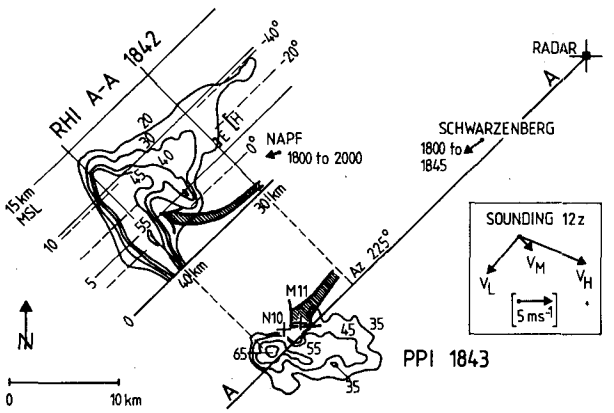

FIG. 20. Radar echo structure of the 6 August 1977 storm. Wind vectors at two stations and winds relative to the storm from the sounding are also indicated. The main updraft is shown schematically by a thick arrow. Note the relatively narrow embryo and hailstone growth range.

is a hybrid between a multicell and a supercell. It has a hook echo at low levels. At mid-levels a WER is present with an extensive overhang. Yet the storm contains multiple centers of activity during its entire lifetime. The strongest inflow region is situated at the rear right-hand flank (see Fig. 21). The PPI's at elevations 5° and 8° as well as the section along A-A show the overhang which reaches reflectivities of 55 dB(Z) at altitudes up to 7.2 km ($T_c = -18$°C). The existence of a broad updraft at the indicated position is supported by two record parachute trajectories of 32 and 36 km. From the radar pattern a two-stage hail formation process can again be inferred. First, hail embryos probably grow in the overhang which extends down to the 0°C isotherm and are then injected into the adjacent organized updraft, where the most favored ones produce the largest hail (see the difference in D_{max} for the collection sites H_1 and H_2 in Table 1). The embryo injection mechanism seems to be very efficient in this storm due to the opposite direction of low and mid-level winds. The storm produced an enormous hailswath with stones with D_{max} up to 45 mm falling during 30 min. The growth ranges of embryos and hailstones indicated in Fig. 21 are relatively narrow. Embryos grow between $-18 \leqslant T_c < -5$°C and hailstones between $-22.6 \leqslant T_c < -2.3$°C. This again is in good agreement with the radar pattern during the growth period.

d. 12 June 1979

The typical radar PPI is shown in Fig. 22, as storm B moved over the seven collection sites, indicated by crosses. Since this storm moved from 208° at 10 m s^{-1}, which is considerably to the *left* of the mean wind in the cloud layer (see winds relative to storm in Fig. 22), the echo can be considered an obstacle to the ambient wind at all levels. The vertical sections constructed from RHI's and PPI's suggest that new growth originates on the left rear flank of the storm and that the reflectivity maxima downwind of that location are progressively lower. Near the rear stagnation point of this multicellular storm, new echos are formed periodically, probably aided by the interaction of the gust front with the low-level westerly wind. The particles are then advected into the main updraft and away from the embryo source region by the upper level westerly wind. With this constellation, no interference between updraft and downdraft and no recirculation of particles is expected.

From isotope data, embryo growth is confined between cloud temperatures of −6.7 and −23.9°C and hailstone growth between −6.3 and −30.5°C (see Section 4 for absolute temperature determination). This is in fair agreement with the radar pattern in Fig. 22 which is admittedly inaccurate due to attenuation problems of the X band RHI's.

e. 7 August 1979

Prefrontal activity in the experimental area triggered a number of cells in the late afternoon. A merger of relatively weak cells produced a storm which by 1820 began traveling from 275° at 7.5 m s^{-1} toward and over the radar site (see wind shift in Fig. 23). The merging of additional cells which were formed on the right forward flank resulted in the propagation of the whole multicellular storm toward the east, although the cloud-layer winds had components predominantly from a southerly direction. The inflow is at the right forward flank (see the RHI at 1824). The radar pattern suggests a tilted updraft undercut by the outflow. Embryos are likely to be produced in the new growth ahead of the main updraft and advected into and over it without large

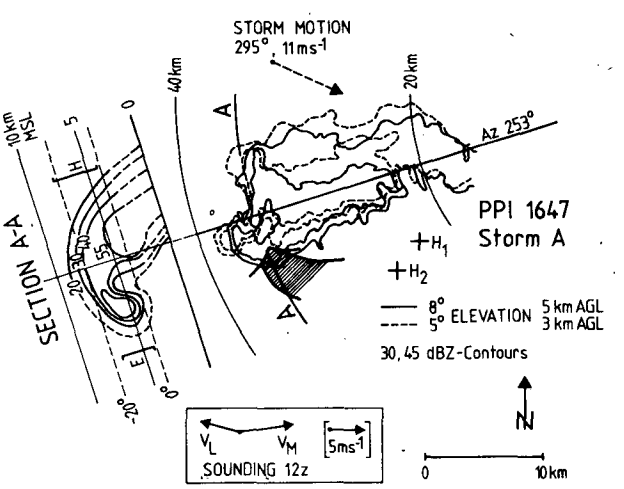

FIG. 21. As in Fig. 20 except for the 14 July 1978 storm. H_1, H_2 are the hail collection sites.

changes in altitude as judged from the persistent 50 dB(Z) contour at 5 km in the RHI's. The larger hailstones are found on hailpads beneath the southern reflectivity maxima which dominate the storm after 1830. Smaller particles are transported further to the north of the storm by the mid and upper tropospheric winds (see Fig. 23). In this storm the embryo and hail growth ranges are equal and confined to the interval −7.2 to −17.8°C, which again is in satisfactory agreement with the RHI pattern.

6. Discussion

Taking all the hailstones that were analyzed for their isotope content, a number of interesting features are observed. In most hailstones the embryos have extreme deuterium values, a fact which had already been noted in earlier analyses (Macklin *et al.*, 1977; Federer *et al.*, 1978; Knight *et al.*, 1981). Of the 78 hailstones, in which more samples than just the embryos themselves were analyzed for the stable isotopes, 63 were at the warm extreme, only 5 at the cold extreme and in 10, the embryo was grown at intermediate temperatures (which originally may have had extreme D-values as well). The relative frequencies of the differences of the D contents of embryos δD_E and δD_{min} (the minimum D content of the day) are plotted in histograms for graupel and frozen drop embryos respectively (Fig. 24). In order to be able to pool the hailstones of different days with different deuterium ranges, all the values were normalized by the ranges R ($=\delta D_{max} - \delta D_{min}$) of each day. The two distributions, whose principal modes are well separated, confirm the earlier observations that graupel and frozen drop embryos have on the average different growth histories.[1]

Of the 61 frozen drop embryos, 90% lie in the warm half of the histogram $[(\delta D_E - \delta D_{min})/R > 0.5]$. The graupel embryos on the other hand, are not necessarily of cold origin. Despite the principal mode lying in the interval 0.2 to 0.3, 44% of the graupel embryos were in the warm half which suggests that riming at low temperatures is often followed by later soaking of the particles.

Concerning the mechanism of formation of the frozen drop embryos, there are three possibilities: coalescence growth of a drop possibly on a large hygroscopic nucleus, melted and recirculated graupel, and drops shed from the surface of existing hailstones. In view of the large number of drop embryos being at the warm extreme of the hailstone layers, we consider the shedding process to be less important. Although in a shedding situation the water film is at 0°C upon disruption, the D content of the drops shed must be close to that of the small droplets which

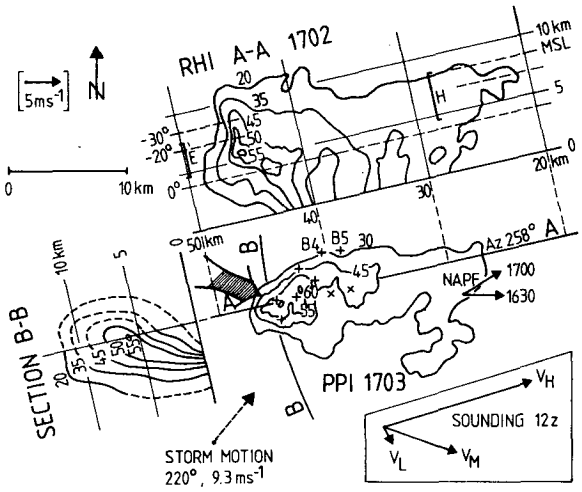

FIG. 22. Radar echo structure of the 12 June 1979 storm. The plus marks are the collection sites from storm B, the crosses are the two collection sites from storm D which passed an hour later (see Table 1). The hailpads B4 and B5 are still outside the 30 dB(Z) contour at 1703.

form the liquid film. The small droplets themselves are in isotopic equilibrium with the environmental vapor. It seems unlikely that this process takes place only at the warm extreme in almost all cases. One would rather expect shedding to occur over the whole temperature range of hailstone growth depending on the water content. The coldest drop embryo, marked with an arrow in Fig. 2, formed at the relatively high temperature of −17.5°C, according to the ICM. Its D content seems to be influenced, however, by that of the opaque cold layer surrounding it.

To distinguish further between the remaining two processes (coalescence and melted/recirculated

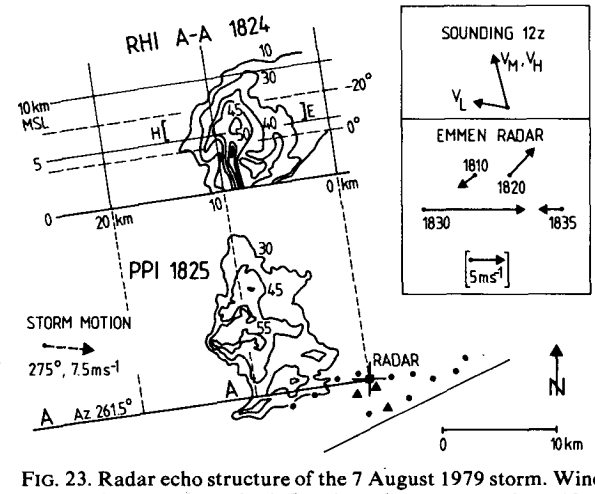

FIG. 23. Radar echo structure of the 7 August 1979 storm. Wind vectors at Emmen show the inflow into the new growth at 1810 and the gust front when the storm passed overhead the radar. Pads with <30 J m^{-2} are indicated by solid dots, those with 30–300 J m^{-2} with triangles. Most hailpads beneath the rest of the echo were not hit.

[1] A Wilcoxon test shows that the two distributions are significantly different at the 1% level.

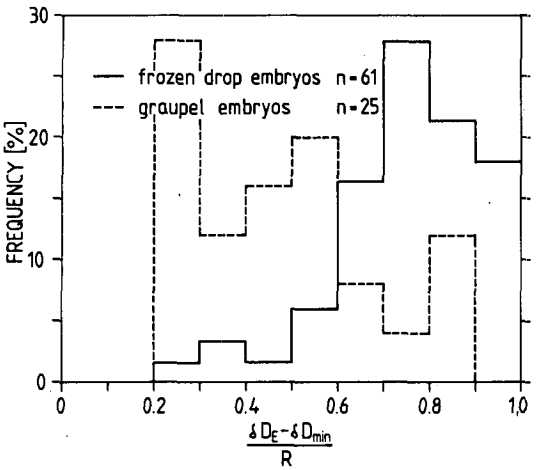

FIG. 24. Frequency distribution of $(\delta D_E - \delta D_{min})/R$ for graupel and frozen drop embryos.

graupel) the degree to which evaporation took place during embryo formation can be used. Since in coalescence an initially small liquid drop grows to raindrop size, the particle is practically always at cloud temperature; thus, a large evaporation effect is not expected. A melted graupel on the other hand, which is already large below the 0°C isotherm will always be warmer than T_c when it is recirculated, since temperature relaxation is slow. Considerable evaporation is therefore expected. An approximate calculation of this evaporation effect leads to the result that at a temperature difference of 1°C, 2.5% of the mass can evaporate during 2 min, yielding a $\Delta\delta O^{18}$ of ~0.4‰. To investigate the situation, the O^{18} enrichment taking place at the surface of the drop embryos is taken as a measure of the amount of evaporation. This enrichment is the deviation of the O^{18}-content of the embryos from the equilibrium line with slope 8.5 in the δD-δO^{18} plot (Fig. 2). The relative frequencies of the enrichment $\Delta\delta O^{18}$ are plotted for graupel and frozen drop embryos separately in the histograms of Fig. 25. It is seen that 33% of the graupel embryos are found in the interval $\sigma(O^{18}) = \pm 0.15$‰, which is the measurement accuracy. Thus a third of those embryos grew without evaporation/condensation taking place. In class 2 (frozen drops), however, only 13% grew without evaporation/condensation, and the large majority of embryos evaporated during their formation. This analysis suggests that the melted graupel mechanism of formation for frozen drop embryos is the more probable one. Other mechanisms can be advanced of course to explain the evaporation effects. If an outer shell of ice is formed on the drop during freezing, which was verified experimentally by many authors (see, e.g., Johnson and Hallett, 1968; Pitter and Pruppacher, 1973), the one described here seems to be the more plausible one. If on the other hand, a slushy mass is formed during freezing of a non-growing drop, rapid evaporation from the surface can set in regardless of the origin of the drop.

An inspection of the radar pictures in Section 5 shows that the typical overhangs which are thought to be the embryo formation regions reach relatively high temperatures at their lower ends where heavy soaking and/or melting can take place. However, typical overhangs are not observed in all hailstorms or they do not reach down to the 0°C isotherm. In view of all these arguments it is difficult to say whether the coalescence or the melted graupel process is the dominant one to produce the frozen drop embryos. It is very probable that both are occurring simultaneously. The presence of some large drops near cloud base is taken into account in the model by setting the autoconversion threshold at the low value of A = 0.5 g kg^{-1}, producing large drops at an early stage (~600 m above cloud base).

A similar analysis has been made for the growth layers. From thick sections crystal size is difficult to infer since they cannot be analysed in polarized light. Therefore the layers of the thick sections used in the stable isotope determinations were separated into clear, transparent and opaque classes. The subjective impressions of two independent analysts of the off-center thin sections (in ordinary and polarized light) of hailstones similar to those analysed for the stable isotopes, indicated that a good correlation between bubble structure and crystal size existed in all collections. In a selected number of the larger hailstones, the crystal size of 323 layers out of a total of 432 layers with known bubble structure could be determined unequivocally. Of those 323 layers 285 or 88% were either clear and transparent with large crystals (>2 mm longest dimension) or opaque with

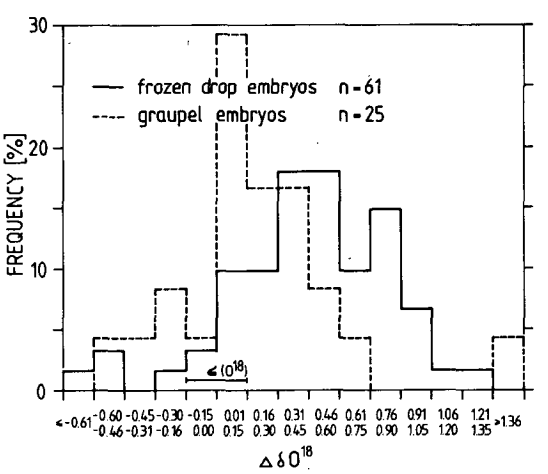

FIG. 25. Frequency distribution of the O^{18} enrichment, $\Delta\delta O^{18}$, for graupel and frozen drop embryos.

small crystals (<0.5 mm); the rest were mainly opaque with large crystals. This high correlation was somewhat surprising, since bubble structure changes are more frequent than crystal size changes due to the more marked dependence of bubble structure on deposit temperature. Reliable simultaneous D and O^{18} determinations were obtained from 244 growth layers. The O^{18} enrichment $\Delta\delta O^{18}$ was calculated and plotted in Fig. 26 as a frequency distribution for the same $\Delta\delta O^{18}$ intervals as for the embryos in Fig. 25. The means and standard deviations for clear and opaque layers are $\Delta\delta O^{18} = 0.66 \pm 0.32$ and $\Delta\delta O^{18} = 0.19 \pm 0.35$, respectively. An inspection of Fig. 26 and a simple R/s-test (range R over standard deviation) indicate that the $\Delta\delta O^{18}$ are approximately normally distributed. A t-test was applied to show that the means are significantly different (at the 1% level). This implies the physical result that, in hailstone growth, opaque layers are grown with less evaporation on the average and often with very little evaporation since the mean $\Delta\delta O^{18}$ lies close to the measurement uncertainty. By measuring the relative isotopic enrichment in O^{18} of opaque layers in the interior of hailstones, it is possible to estimate the extent of soaking effects. This could well serve as an additional piece of evidence to deduce approximate liquid water contents in hailclouds according to the scheme given by Macklin (1977). Clear layers grow under wet growth conditions most of the time, with a water film on their surface undergoing appreciable evaporation. The D content of the clear layers therefore seldom corresponds to that of the droplets responsible for the accretion because of the kinetic effect. In attributing an absolute temperature scale to the deuterium measurements the slight correction for non-equilibrium was applied to those layers. Otherwise the calculated trajectories are generally too low, indicating growth at too high a temperature. The trajectories for all the hailstones, which are deduced from the isotope data in conjunction with the ICM, correspond nicely with the radar data. The large height variations during growth and the resulting excessive updraft speeds obtained by Macklin *et al.* (1970) and Jouzel *et al.* (1975) are substantially reduced. Rather it appears that hailstone growth is confined to a "balance level" in a relatively narrow temperature interval; this is especially observed in larger hailstones (Figs. 10 and 13). At these levels, the largest updrafts with the highest liquid water contents are expected. On the other hand, Fig. 20 suggests that hailstones were transported up to the −40°C isotherm and higher, but in the hailstones analyzed there is no evidence of this part of the trajectory, since apparently there was no growth below −23°C. However, the temperature ranges E and H, indicated in Figs. 18–23, are those found for the limited samples analyzed. It is evident from these figures

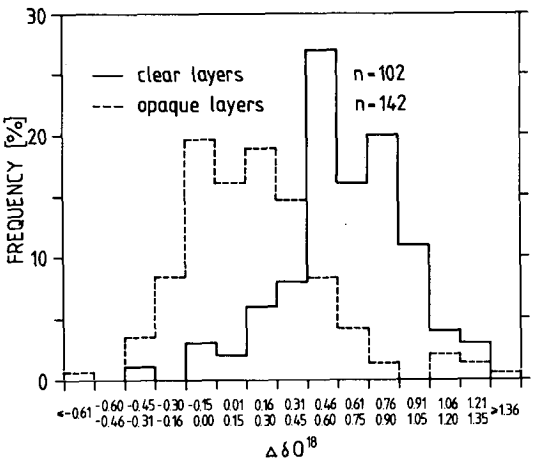

FIG. 26. Frequency distribution of the O^{18} enrichment, $\Delta\delta O^{18}$, for clear and opaque hailstone growth layers.

and Table 1 that the smallest sample of 080677 ($N = 10$) has the smallest embryo and hailstone growth ranges, 4.4 and 9.2°C, respectively, while in the largest sample on 061279 ($N = 33$), these ranges were 17.2 and 24.2°C, respectively. It would be interesting to see, whether these ranges, calculated with the ICM of course, would become larger in a still larger collection.

7. Conclusions

Hailstone collections were made in seven different storms with good radar coverage. Thin sections of over 2000 hailstones were classified according to embryo type, and it was shown that frozen drops were dominant. A total of 86 hailstones were also analyzed for their isotope content. The deviations δD and δO^{18} of embryos and growth layers from standard mean ocean water (SMOW) were determined simultaneously. A large majority of frozen drop embryos had δD values at the warm extreme (highest δD of the entire hailstone). Statistical tests showed that frozen drop embryos grow at significantly warmer temperatures than graupel embryos. The frequency distribution of the ratio $(\delta D_E - \delta D_{min})/R$ for the graupel is, however, appreciably skewed toward relatively warm embryos (Fig. 2). This indicates that many graupel embryos were soaked and/or partially melted at higher temperatures after their formation.

The deviation of δO^{18} from the equilibrium line ($\Delta\delta O^{18}$) was also significantly larger for the frozen drops which means that they evaporated more than those classified as graupel. Since evaporation is strongest if a large particle is ascending in an updraft, where it is considerably warmer than its surroundings, these facts suggest that some frozen drop embryos probably originate from melted and recirculated aggregates and graupel. A few "transition"

embryos, with indications of soaking/melting as the one shown in Fig. 15, support this hypothesis. This will be tested more quantitatively using a model, currently being developed in our laboratory, which includes temperature and isotopic relaxation effects for individual drops which are recycled from cloud base. A first result shows that the evaporation effect is strong if the drop/melted graupel ascends without collecting droplets, otherwise it is largely masked.

The frequency distribution of $\Delta\delta O^{18}$ for the growth layers showed a significant difference between clear and opaque layers as well, indicating that clear layers largely grow under non-equilibrium conditions with considerable evaporation from their surfaces. Tangential variations of δD, δO^{18} and $\Delta\delta O^{18}$ in clear layers were not very large.

A comparison was made between isotopic data of hailstones interpreted either on the basis of the adiabatic model (AM) or the isotopic cloud model (ICM) presented in Part I. Both models rely on assumptions which are sometimes difficult to justify, but the ICM takes mixing, depletion, fallout, raindrops and ice into account. The determination of growth trajectories based on the ICM shows that they are in agreement with the deductions obtained from crystallography of the hailstones and with the morphology of the radar echos. For embryo growth, a range between -5 and -24°C was obtained, with most of the frozen drop embryos growing at the warm extreme. Using the ICM the most common growth temperatures for all layers were between -15 and -25°C. This is plausible, since in this region the largest updrafts with high LWC are expected and the precipitation load is not yet very large. It must be remembered, however, that the D ranges obtained are dependent on sample size. The largest range of hailstone growth temperatures for a particular day was observed on 061279. On this day 33 hailstones were analyzed for isotopes, whereas on the day with the smallest range in growth temperatures (080677), only 10 hailstones were investigated.

In hailstone growth, the large height deviations obtained with the AM are considerably reduced if the ICM is used, which eliminates the obvious difficulty of growth at or below -40°C. For the 86 hailstones investigated on 5 days the overall growth range lies between -2.5 and -30.5°C for the ICM, whereas for the AM it extends down to -50°C, if no change in the deuterium concentration δ_0 of the subcloud vapor is assumed (Figs. 10–14). Measurements of δ_0 as a function of altitude (0.4–2.1 km) showed, however, that the vertical, horizontal and temporal variations of δ_0 in the experimental area can be as large as 10–15‰, even on days with no precipitation. In the samples taken in the inflow of thunderstorms, however, the vertical gradient was substantially reduced. The inconstancy of δ_0 has the effect of shifting the isotope profiles without changing their shape. This may lead to growth temperatures for the hailstone layers which are inconsistent with deductions from other sources. The crystallographic method for determining δ_0 is therefore preferred, where a temperature of -15°C is attributed to the richest small crystalline layer and -24°C to the poorest layer with large crystals (Macklin, 1977). It was possible to use this method with the thick sections, since the correlation between clear and large crystalline and opaque and small crystalline growth layers was high.

Acknowledgments. This work was financed within the Grossversuch IV hail suppression experiment. The contributions of all the participants in this experiment are gratefully acknowledged. Special thanks are due to Dr. Charles Knight for a very thorough and helpful review and to Dr. A. Waldvogel for the numerous discussions during the course of this work.

REFERENCES

Ashworth, E., T. Ashworth and C. A. Knight, 1980: Cylindrical ice accretions as simulations of hail growth: III. Analysis techniques and application to trajectory determination. *J. Atmos. Sci.*, **37**, 846–854.

Browning, K. A., and G. B. Foote, 1976: Airflow and hail growth in supercell storms and some implications for hail suppression. *Quart. J. Roy. Meteor. Soc.*, **102**, 499–533.

Cloud Physics Group ETH, 1980: Projekt Grossversuch IV. Bericht über das Feldexperiment im Napfgebiet. *Wiss. Mitteilung*, No. 84, Eidg. Hagelkommission, 275 pp. [Atmospheric Physics ETH, Zurich 8093, Switzerland].

Craig, H., 1961: Isotopic variations in meteoric waters. *Science*, **133**, 1702–1703.

Dansgaard, W., 1964: Stable isotopes in precipitation. *Tellus*, **16**, 436–468.

Ehhalt, D. H., 1974: Vertical profiles of HTO, HDO and H_2O in the troposphere. NCAR Tech. Note TN/STR-100, 131 pp. [NTIS PB 245731/AS].

Federer, B., J. Jouzel and A. Waldvogel, 1978: Hailstone trajectories determined from crystallography, deuterium content and radar backscattering. *Pure Appl. Geophys.*, **116**, 112–129.

——, A. Waldvogel, W. Schmid, F. Hampel, E. Rosini, D. Vento, P. Admirat and J. F. Mezeix, 1979: Plan for the Swiss randomized hail suppression experiment, design of Grossversuch IV. *Pure Appl. Geophys.*, **117**, 548–571.

Heymsfield, A. J., A. R. Jameson and H. W. Frank, 1980: Hail growth mechanisms in a Colorado storm: Part II. Hail formation processes. *J. Atmos. Sci.*, **37**, 1779–1807.

Johnson, D. A., and J. Hallett, 1968: Freezing and shattering of supercooled water drops. *Quart. J. Roy. Meteor. Soc.*, **94**, 468–482.

Jouzel, J., L. Merlivat and E. Roth, 1975: Isotopic study of hail. *J. Geophys. Res.*, **80**, 5015–5030.

——, and L. Merlivat, 1980: Growth regime of hailstones as deduced from simultaneous D and O^{18} measurements. *Commun. 8ème Conf. Int. sur la Physique des Nuages*, Clermont-Ferrand, 253–256 [L.A.M.P., P.O. Box 45, Aubière, 63170, France].

Knight, C. A., and N. C. Knight, 1970: Lobe structures of hailstones. *J. Atmos. Sci.*, **27**, 667–671.

——, D. H. Ehhalt, N. Roper and N. C. Knight, 1975: Radial and tangential variation of deuterium in hailstones. *J. Atmos. Sci.*, **32,** 1990–2000.

——, N. C. Knight and K. A. Kime, 1981: Deuterium contents of storm inflow and hailstone growth layers. *J. Atmos. Sci.*, **12,** 2485–2499.

Knight, N. C., and M. English, 1980: Patterns of hailstone embryo type in Alberta hailstorms. *J. Rech. Atmos.*, **14,** 325–332.

Levi, L., and A. N. Aufdermaur, 1970: Crystallographic orientation and crystal size in cylindrical accretions of ice. *J. Atmos. Sci.*, **27,** 443–452.

Macklin, W. C., 1977: The characteristics of natural hailstones and their interpretation. *Hail: A Review of Hail Science and Hail Suppression*, G. B. Foote and C. A. Knight, Eds., *Meteor. Monogr.*, No. 38, Amer. Meteor. Soc., 65–86.

——, L. Merlivat and C. M. Stevenson, 1970: The analysis of a hailstone. *Quart. J. Roy. Meteor. Soc.*, **96,** 472–486.

——, C. A. Knight, H. E. Moore, N. C. Knight, W. Pollock, J. N. Carras and S. Thwaites, 1977: Isotopic, crystal and air bubble structures of hailstones. *J. Atmos. Sci.*, **34,** 961–967.

Merlivat, L., and J. Jouzel, 1979: Global climatic interpretation of the D-O^{18} relationship for precipitation. *J. Geophys. Res.*, **84,** 5029–5033.

Nelson, S. P., 1980: Hail production in a supercell-type storm. *Proc. 3rd WMO Sci. Conf. Weather Modification*, Clermont-Ferrand, 655–661.

Newton, C. W., and J. C. Fankhauser, 1964: On the movements of convective storms, with emphasis on size discrimination in relation to water-budget requirements. *J. Appl. Meteor.*, **6,** 651–668.

Pitter, R. L., and H. R. Pruppacher, 1973: A wind tunnel investigation of freezing of small water drops falling at terminal velocity in air. *Quart. J. Roy. Meteor. Soc.*, **99,** 540–550.

Roos, D. v. d. S., H. Schooling and J. C. Vogel, 1977: Deuterium in hailstones collected on 29 November 1972. *Quart. J. Roy. Meteor. Soc.*, **103,** 751–767.

Waldvogel, A., B. Federer and P. Grimm, 1979: Criteria for the detection of hail cells. *J. Appl. Meteor.*, **18,** 1521–1525.